Geophysical Research Letters

RESEARCH LETTER
10.1029/2018GL077882

Seminal Evidence of a 2.5-Sol Ultra-Fast Kelvin Wave in Mars' Middle and Upper Atmosphere

Federico Gasperini[1], **Maura E. Hagan**[1], **and Jeffrey M. Forbes**[2]

[1]Department of Physics, Utah State University, Logan, UT, USA, [2]Ann and H.J. Smead Department of Aerospace Engineering Sciences, University of Colorado Boulder, Boulder, CO, USA

Key Points:
- A 2.5-sol ultra-fast Kelvin wave (UFKW) is a dominant global-scale feature of Mars' middle and upper atmosphere at low latitudes
- Secondary waves (SWs) arising from UFKW-tidal interactions represent an important source of variability in the aerobraking region
- The UFKW is confined to low latitudes and is quasi equatorially symmetric, while the SWs extend up to midlatitudes and display asymmetries

Correspondence to:
F. Gasperini,
gasperini@usu.edu

Citation:
Gasperini, F., Hagan, M. E., & Forbes, J. M. (2018). Seminal evidence of a 2.5-sol ultra-fast Kelvin wave in Mars' middle and upper atmosphere. *Geophysical Research Letters*, *45*, 6324–6333. https://doi.org/10.1029/2018GL077882

Received 12 MAR 2018
Accepted 6 JUN 2018
Accepted article online 19 JUN 2018
Published online 4 JUL 2018

Abstract The structure and dynamics of Mars' middle and upper atmosphere is significantly impacted by waves propagating from the lower atmosphere. Using concurrent temperature and neutral density measurements taken by the Mars Reconnaissance Orbiter and Mars Atmosphere and Volatile EvolutioN satellites, we demonstrate for the first time that a 2.5-sol ultra-fast Kelvin wave is a prominent global-scale feature of the low-latitude middle (i.e., 30–80 km) and upper (approximately 150 km) atmosphere of Mars. Further, we present evidence of secondary waves arising from nonlinear interactions between this ultra-fast Kelvin wave and solar tides, and based on their amplitudes we surmise that they could represent an important source of tidal and longitudinal variability in the aerobraking region.

Plain Language Summary The upper atmosphere of Mars is driven by a combination of effects linked to solar radiation and to waves that originate in the lower and middle atmosphere. Upward propagating waves are responsible for short-term temperature and wind variations in Mars' middle and upper atmosphere and couple different layers of Mars' atmosphere. While in the last couple of decades our understanding of the processes responsible for this coupling has considerably improved, there are many unresolved questions regarding the impacts of the entire spectrum of these waves on the upper atmosphere of Mars. In this work we demonstrate that a strong ultra-fast Kelvin wave with a period of 3 sols and the secondary waves generated by its nonlinear interaction with solar tides can be a large source of variability in Mars' middle and upper atmosphere.

1. Introduction

The upper atmosphere of Mars is strongly impacted by solar radiative forcing, the solar wind, dust storms, and dynamical coupling due to waves propagating from the lower atmosphere, including gravity waves, planetary waves (PWs), and tides (e.g., Bougher et al., 2008; Forbes, 2002; Jakosky et al., 2017). These atmospheric waves transport momentum and energy from the lower atmosphere to the middle and upper atmosphere, where they are a primary driver of sol-to-sol, intraseasonal, and seasonal variability. Evidence for wave coupling into the upper atmosphere of Mars was previously diagnosed in atmospheric density measurements in the 100- to 150-km region derived from accelerometer data (e.g., Moudden & Forbes, 2015; Wang et al., 2006; Withers et al., 2003), numerical modeling studies (e.g., Angelats i Coll et al., 2004; Forbes et al., 2002; Moudden & Forbes, 2008), Mars Global Surveyor radio occultation data (e.g., Cahoy et al., 2006), and Mars Atmosphere and Volatile EvolutioN (MAVEN) measurements (e.g., England et al., 2016; Liu et al., 2017).

To date, most studies have examined the vertical wave coupling at Mars in the context of specific eastward-propagating diurnal solar tides, commonly referred to as diurnal Kelvin waves (e.g., DKWs; Forbes & Hagan, 2000; Forbes et al., 2001; Guzewich et al., 2012; Wilson, 2000). In classical atmospheric wave theory (e.g., Longuet-Higgins, 1968), Kelvin waves (KWs) are the first symmetric eastward-propagating gravity-type modes and are equatorially trapped. In Earth's atmosphere, KWs also play an important role, with the shorter-period (2–6 days) *ultra-fast* Kelvin waves (UFKWs) extending into the thermosphere. In this work we present first evidence for UFKWs in Mars' atmosphere and demonstrate that they effectively couple the middle atmosphere to the thermosphere.

Our experimental evidence for UFKW vertical coupling is obtained from Mars Climate Sounder (MCS) temperature measurements from the Mars Reconnaissance Orbiter (MRO) between 30–80 km and neutral densities from the accelerometer on board the MAVEN satellite near 130–170 km during four periods when MAVEN

©2018. American Geophysical Union. All Rights Reserved.

sampled the equatorial region. Particular focus is placed on a 18-sol period near autumnal equinox, when the wave signatures are most prominent. Using the approach of Moudden and Forbes (2010, 2011a, 2011b), we present evidence of secondary waves arising from nonlinear interactions between this UFKW and solar tides. The following section describes the MRO/MCS and MAVEN data, section 3 describes the methodology, section 4 presents the results, while section 5 provides a summary and conclusions.

2. Data

The data used in this study consist of temperature profiles (version 4) from the MCS instrument on board MRO covering altitudes between ~20 and ~80 km and MAVEN accelerometer-derived neutral densities (level 3) near periapsis (i.e., ~130–170 km). The MCS temperature data are from the Derived Data Record archive available at the Planetary Science Database (http://pds-atmospheres.nmsu.edu/), while the MAVEN neutral density data are from the Science Data Center at the Laboratory for Atmospheric and Space Physics (https://lasp.colorado.edu/maven/sdc). This work focuses on the period between 1 November 2014 and 31 April 2017, when concurrent MCS and MAVEN data are available. This period consists of 888 sols starting at solar longitude $L_s = 224.8$ and ending at $L_s = 357.1$, and covering ~1.33 Martian years.

MCS is a limb-scanning infrared radiometer that launched aboard MRO and became fully operational at the end of September 2006 (McCleese et al., 2007). MRO's orbit is nearly polar and Sun-synchronous with an inclination of 92.66° . At any given time the spacecraft's local time (LT) is near 15 LT or 3 LT during the ascending or descending parts of the orbit, respectively, except poleward of 75° latitude where the spacecraft shifts from 15 LT or 3 LT and vice versa in the opposite polar hemisphere. The orbital period is 112 min translating to nearly 13 passages per sol. Each orbit is shifted by about 27° in longitude from the earlier orbit. The vertical resolution of the MCS data is ~5 km with horizontal resolution of ~150–300 km, depending on altitude. The uncertainty in MCS temperature measurements is ~0.4 K (i.e., 0.25% of average temperature) between 5 to 300 Pa (i.e., 20–80 km). Closer to the surface the errors are ~0.5 to 3 K (0.5 to 3%), while above 5 Pa the errors steadily increase to ~10 K near 0.06 Pa, that is, ~80 km (Guzewich et al., 2012).

MAVEN was launched in November 2013 and entered Mars' orbit on 21 September 2014. After a 2-month transition phase, MAVEN entered the nominal science orbit, an elliptical orbit around Mars at 75° inclination, with a 4.5-hr period and periapsis altitude of ~130–170 km (density corridor of 0.05–0.15 kg/km^3). Periapsis precesses over a wide range of latitudes and local times. During each sol MAVEN samples 5 to 6 Mars' longitudes and precesses through ~3.5 diurnal cycles every Martian year (i.e., 24-hr local time coverage occurs in about 200 sols). An in-depth review of MAVEN and its mission is provided by Jakosky et al. (2015). During the nominal science orbit, when periapsis altitude is near 160 km, the onboard accelerometer provides a data source for determining atmospheric density (Zurek et al., 2015). The ability to recover density depends strongly on orbit and spacecraft conditions. Nonrandom errors can be introduced in the conversion of accelerations to density by uncertainties in spacecraft attitude and in the associated aerodynamic error coefficients. Zurek et al. (2017) compared densities from different spacecraft attitudes and for different satellite passes and reported accuracies of a few percent, while comparisons also made by Zurek et al. (2017) using tracking data and variations in spacecraft velocity indicate systematic errors of less than 10%.

3. Methodology

3.1. Normalizing MAVEN Densities to 150 km

Zurek et al. (2017) recently performed analysis of MAVEN accelerometer-derived total mass densities, deriving a scale height varying linearly with height and referenced to 150 km. To facilitate analysis of wave signatures, we adopt the Zurek et al. (2017) approach and normalize MAVEN neutral densities between 130 and 170 km to a reference height of 150 km. Note that noninfinite vertical wavelengths will add some uncertainty (or inherent averaging) to the normalized data, but analysis of various waves in the Mars Climate Database (Forget et al., 1999; Millour et al., 2015) data by us (not shown) suggests that this effect is likely to be small between 130 and 170 km.

Assuming that the scale height (H) varies linearly with height in this range, the density ρ_0 at the reference height $z_0 = 150$ km is related to the density at any height $z = 130$–170 km by the expression:\vspace*{0pt}

$$\rho_0 = \rho \frac{H}{H_0} e^{-\int_z^{z_0} \frac{dz}{H}}, \tag{1}$$

where H_0 is the scale height at z_0. For H we adopt the expression obtained by Zurek et al. (2017) by linearly fitting MAVEN periapsis densities above 150 km to periapsis altitude (h_r) and solar zenith angle (SZA):

$$H = 10.2 + 2.3\cos(\mathrm{SZA}) + 0.1h_r, \tag{2}$$

and note that the variation with height of H remains linear for altitudes as low as 130 km (see the first panel of Figure 8 in Zurek et al. (2017)). Using the identity

$$\int \frac{dz}{a+bz} = \frac{1}{b}\ln(a+bz) \tag{3}$$

and expressing h_r in equation (2) as $h_r = z - 150$, equation (1) can be written as

$$\rho_0 = \rho\left(\frac{H}{H_0}\right) e^{\frac{1}{0.1}\left[\ln\left(\frac{H}{H_0}\right)\right]} = \rho\left(\frac{H}{H_0}\right) e^{\left[\ln\left(\frac{H}{H_0}\right)\right]^{10}} = \rho\left(\frac{H}{H_0}\right)^{11}, \tag{4}$$

which, using the expression of H in equation (2), is equivalent to

$$\rho_0 = \rho\left(1 + \frac{0.1(z-150)}{10.2 + 2.3\cos(\mathrm{SZA})}\right)^{11}. \tag{5}$$

Equation (5) is used to normalize MAVEN periapsis densities between 130 and 170 km to a constant altitude of 150 km. During the 888-sol period analyzed, MAVEN mean periapsis height is 153.4 km with over 89% of the data points within the 130- to 170-km altitude range. Densities outside of this interval are treated as missing data. [Note that some sensitivity to the exponent in equation (5) was found for altitudes greater than ~165 km; thus, caution is warranted if using equation (5) to normalize densities above ~165 km.]

3.2. Fitting of MAVEN Densities to a Proxy for Solar Irradiance at Mars

In order to estimate the impact of thermospheric in situ solar forcing on observed MAVEN densities, we invoke a proxy for extreme ultraviolet (EUV) solar irradiance based upon an adjusted 10.7-cm solar radio flux (designated as adj-F10.7). Because Mars has only a weak remnant magnetic field (e.g., Breus & Krymskii, 2017), we do not have to account for magnetic variations in this analysis. We estimate solar fluxes received at Mars following the method of Forbes et al. (2006). Briefly, we assume that solar flux varies inversely with distance from the Sun squared and is shifted in time from what is observed at Earth using the Earth-Sun-Mars angle and a 27-day solar rotation period.

We quantify and remove neutral density variability due to in situ solar forcing using a technique analogous to that of Gasperini et al. (2015) who analyzed Gravity Field and Steady State Ocean Circulation Explorer satellite neutral densities and winds in Earth's thermosphere at ~260 km. We use linear regression to fit MAVEN zonal mean (ZM) densities to the adj-F10.7 on 90-sol windows, stepping forward 1 sol at the time. A 90-sol window is chosen in order to capture any significant solar flux variability in the 60- to 90-sol range. Zonal (i.e., longitudinal) means are calculated on 3-sol sliding windows, which provide the longitude coverage necessary to compute accurate ZMs. We then remove these fits from the raw density data and analyze the resulting residuals (hereafter referred to as density residuals) for wave content. (Note that while MAVEN provides in situ EUV measurements, our study only implements adj-F10.7 values for the purpose of demonstrating that there is little solar-related variability at periods <23 sols.)

Figure 1a shows MAVEN ZM densities normalized to 150 km, daily adj-F10.7 values calculated as described above, and 90-sol running fits of the densities to the adj-F10.7. The fits only capture a fraction of the temporal variability observed in the ZM densities (up to ~30% or ~0.06 kg/km^3). This is not surprising since we expect the majority of the sol-to-sol variability in Mars' thermospheric densities to be generated by upward propagating waves. In order to investigate the temporal variability in the ZM densities and solar flux, Figure 1c shows the periodogram of adj-F10.7 and MAVEN ZM densities before and after the removal of the fits (hereafter referred to as MAVEN residuals). The ZM densities display significant periodicities around 2 to 30 sols, while the ZM density residuals lack the dominant ~26-sol solar rotation variation found in the ZM densities. Figure 1b shows solar longitude L_s as function of sol for the period analyzed. Separate analysis of column dust data retrieved from Thermal Emission Imaging System camera on board the Mars Odyssey orbiter (not illustrated) shows lack of any significant (>95% confidence level) periodicity between 2 and 23 sols. Thus, the majority of the temporal variability in MAVEN ZM density shown in Figure 1c is not ascribable to solar or dust

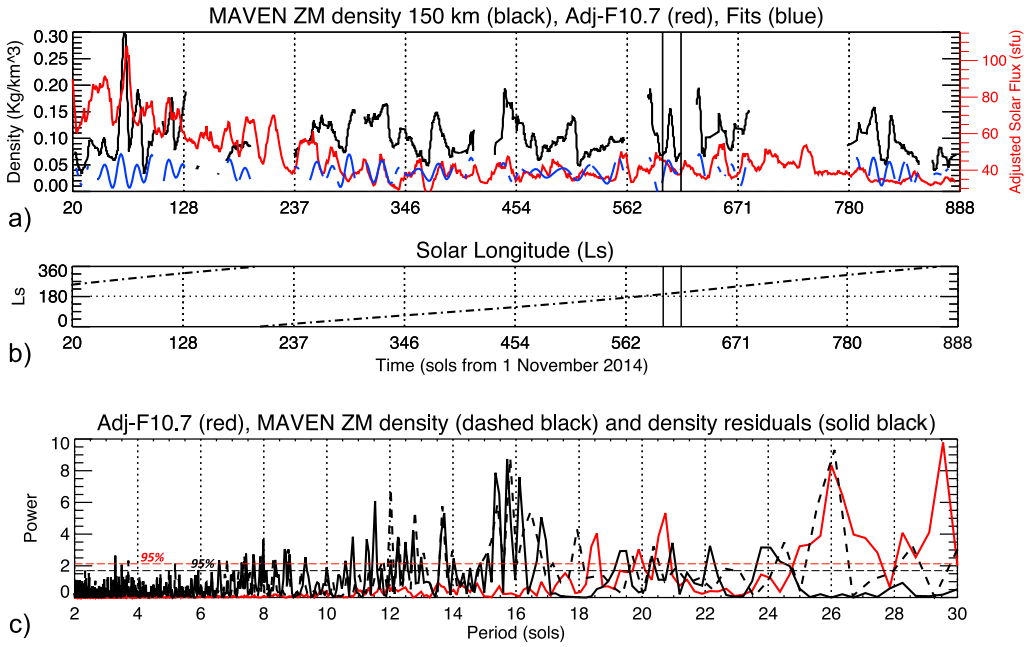

Figure 1. (a) Time series of Mars Atmosphere and Volatile EvolutioN (MAVEN) zonal mean (ZM) density normalized to 150 km (black curve), adj-F10.7 (red curve), and least squares fits between them (blue curve) during the 888-sol period between 1 November 2014 and 31 April 2017. (b) Solar longitude (L_s) for the 888-sol period shown in panel a. (c) Periodogram of MAVEN ZM density (black dashed curve), MAVEN density residuals (black solid curve), and adjusted-F10.7 (red curve). Density residuals clearly lack the solar rotation variation around 26 sols. The black vertical lines in panels a and b indicate the 18-sol period between sol 597 and sol 615 that is the focus of this study.

forcing and ought to be explained by the effect of upward propagating waves (e.g., zonally symmetric, i.e., $s = 0$, oscillations due to dissipation of tides that are modulated at PW periods, i.e., 3–20 sols. See Forbes et al., 2018, for more details.)

3.3. Investigating Nonlinear Interactions Using Pseudolongitudes

Tides, Kelvin waves, and PWs can interact nonlinearly creating secondary waves (SWs) that add significant spatial-temporal variability to the upper atmosphere (Moudden & Forbes, 2010, 2011a, 2011b). The process of nonlinear interaction between global-scale waves, including tides, PWs, and UFKWs, occurs through a nonlinear quadratic interaction that results in the generation of sum and difference SWs (Teitelbaum & Vial, 1991). Numerical simulations (Palo et al., 1999) and observations (Moudden & Forbes, 2013) focused on the terrestrial atmosphere suggest that SWs propagate away from their sources as independent oscillations. Each SW is affected differently by the background wind field and dissipation (e.g., Gasperini, Forbes, & Hagan, 2017).

In order to investigate the presence of UFKW-tide interactions in Mars atmosphere, we employ the method developed by Moudden and Forbes (2010, 2011a, 2011b) and successfully applied by Gasperini et al. (2015) and Gasperini, Forbes, Doornbos, and Bruinsma (2017) to diagnose waves in Earth's atmosphere. The methodology consists of ordering data in pseudolongitudes, the traditional longitude incremented by 360° times the number of Mars revolutions relative to a given time. This arrangement eliminates the fictitious discontinuity at 0/360° longitude. Pseudolongitude λ_p is defined from the traditional longitude λ as $\lambda_p = \lambda + 2\pi c$ where c denotes the number of completed cycles (i.e., the number of sols elapsed since the start of the data series). The equivalency between time and pseudolongitude derives from the fact that the orbit is Sun-synchronous. As such a configuration: $t = t_{LT} + \lambda_p \times sol/2\pi$ where t and t_{LT} are the UT and local times, respectively. We refer the reader to Moudden and Forbes (2010) for additional details. Spectral analysis of a given time series of space-based measurements, as described above, reveals the periodicities of the dominant tides, UFKWs, PWs, and any wave-wave modulations. Nonmigrating (i.e., non–Sun-synchronous) tides appear as integers, while sidebands peaks arising from nonlinear interactions are located at decimal values.

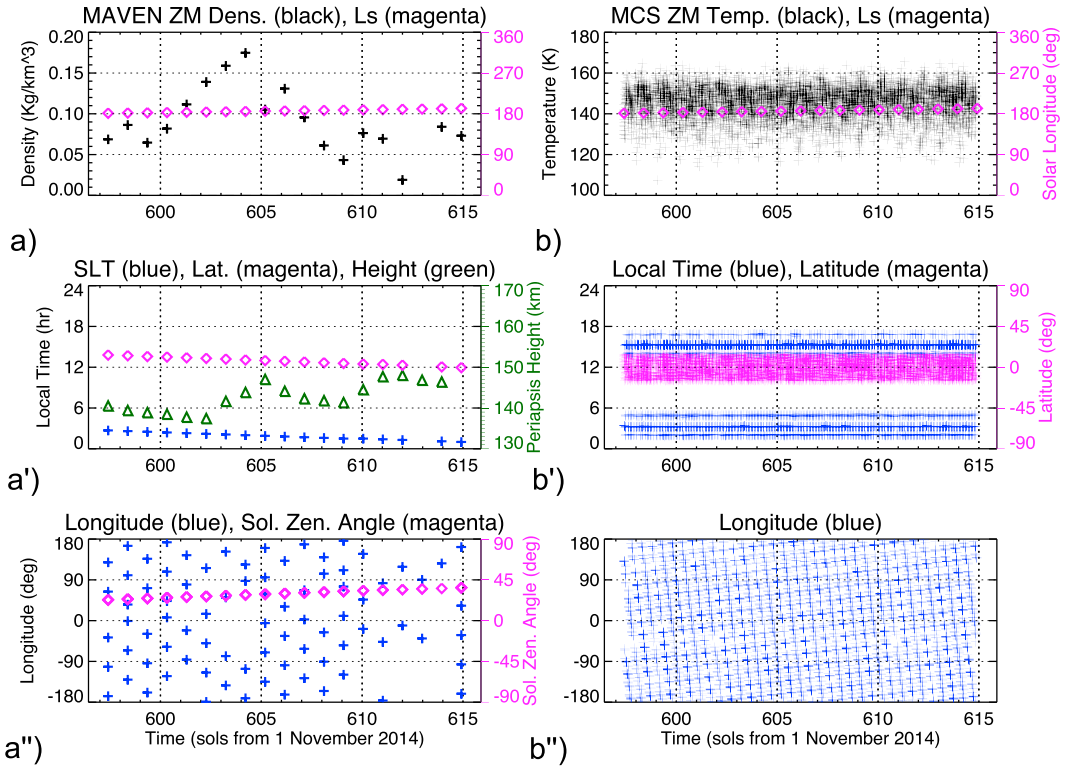

Figure 2. (a and b) Mars Atmosphere and Volatile EvolutioN (MAVEN) zonal mean (ZM) density residuals at 150 km and Mars Reconnaissance Orbiter (MRO)/Mars Climate Sounder (MCS) ZM temperatures at 80 km (*plus* symbols in black), and Ls (*diamond* symbols in magenta) during sol 597–615. (a′ and b′) MAVEN and MRO local time (*plus* symbols in blue) and latitude (*diamond* symbols in magenta), and MAVEN perithe wave-3 structure,apsis altitude (*triangle* symbols in green). (a″ and b″) MAVEN and MRO longitude (*plus* symbols in blue) and MAVEN solar zenith angle (*diamond* symbols in magenta).

4. Results

MAVEN's latitudinal precession is such that periapsis is within ±15° latitude during four ~40-sol intervals between November 2014 and April 2017, including sols 141–180, 371–411, 597–634, and 833–872 referenced from 1 November 2014. Hereafter, we focus on the 18-sol period between sol 597 (L_s = 181.3°) and sol 615 (L_s = 192.0°) near autumnal equinox. Figure 2 shows MAVEN ZM density residuals normalized to 150 km and MRO/MCS ZM temperatures and their orbital parameters for this period, when the local time associated with the MAVEN orbit varies between ~1 and 2 LT, its periapsis altitude varied between 137.4 and 148.0 km (mean of 142.6 km), and latitude between 15.0° N and 0.1° S. The corresponding MRO orbit local time varies between ~2 and 5 LT on one side of the orbit and between ~14 and 17 LT on the other. As shown in panels *a*″ and *b*″, MAVEN samples 5 to 6 longitudes at a single latitude every sol, while MCS samples a range of longitudes and latitudes up to ~ ±87°. By confining the analysis to such a short interval, we can avoid convolving data from multiple seasons and assume that MAVEN measurements are made at a constant local time (N.B., MAVEN precesses by ~2.0 hr in 18 sols.)

Spectral analyses of MCS temperatures at 80 km and MAVEN densities at 150 km reveal the existence of a prominent 2.5-sol periodicity in Mars' middle and upper atmosphere. The periodograms of MAVEN ZM removed (hereafter ZMR) density residuals at 150 km (Figure 3a) and MCS ZMR temperatures at 80 km (Figure 3b) show dominant 2.5-sol periodicities. Analysis of Thermal Emission Imaging System column dust data (not illustrated) shows low dust levels (<0.19 of infrared absorption of column dust optical depth at 9.3 μm) and absence of any 2.5-sol periodicity in dust opacity during sols 597–615. Thus, we conclude that this 2.5-sol wave is likely not associated with dust effects. The period versus zonal wavenumber spectra of MAVEN ZMR density residuals (Figure 3*a*′) and MCS ZMR temperatures (Figure 3*b*′) demonstrate that the 2.5-sol periodicity is eastward propagating and possesses zonal wavenumber -1 and thus is the signature of a UFKW. Furthermore, the presence of this periodicity at both heights suggests that the UFKW is propagating from 80 to 150 km. The UFKW is found to possess amplitudes up to 6 K at 80 km and 20 g/km^3 at 150 km. Other waves

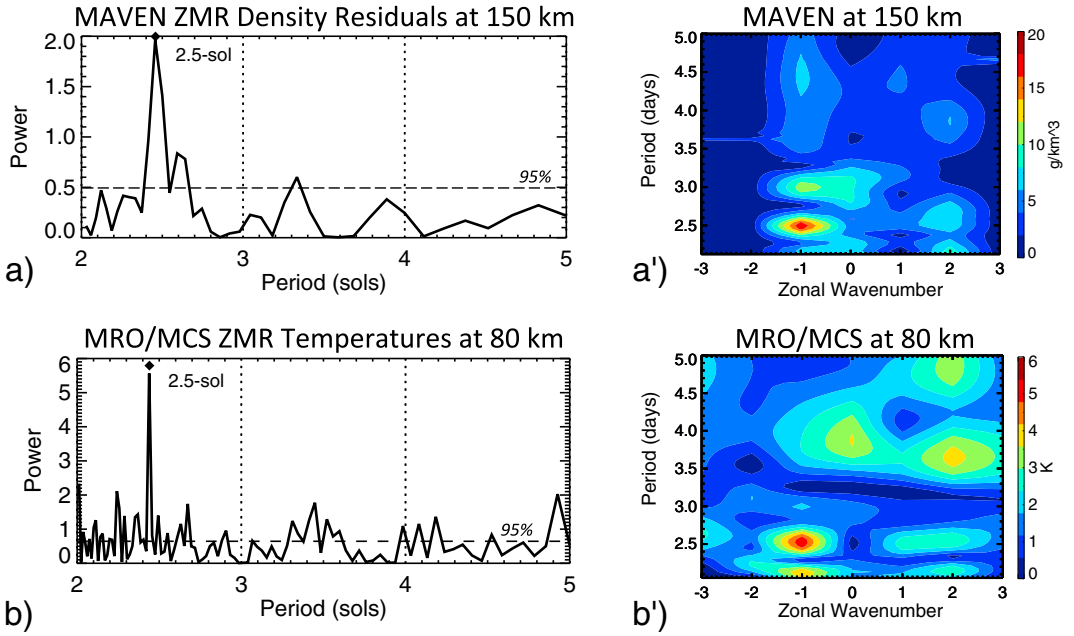

Figure 3. Periodograms of Mars Atmosphere and Volatile EvolutioN (MAVEN) ZMR density residuals at 150 km (panel a) and Mars Reconnaissance Orbiter (MRO)/Mars Climate Sounder (MCS) ZMR temperatures at 80 km (panel b) averaged around the equator (±15° latitude) for sols 597–615. The periodograms reveal a dominant 2.5-sol periodicity at both 80 and 150 km. The corresponding period versus zonal wavenumber plots for MAVEN and MCS are shown in panels a′ and b′, respectively. The 2.5-sol periodicity is eastward propagating and has $s = -1$ and thus is the signature of a ultra-fast Kelvin wave. The ultra-fast Kelvin wave displays amplitudes up to 6 K at 80 km and up to 20 g/km^3 at 150 km.

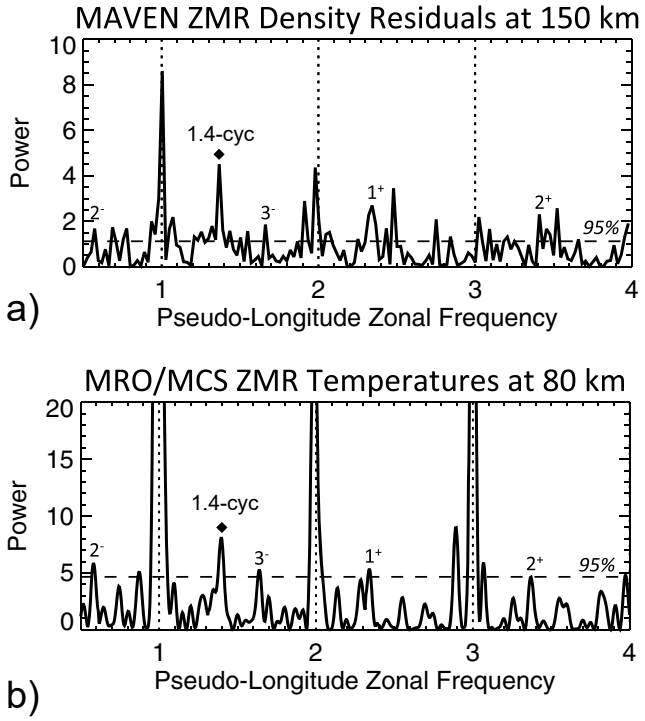

Figure 4. Pseudolongitude spectra of Mars Atmosphere and Volatile EvolutioN (MAVEN) ZMR density residuals at 150 km (panel a) and Mars Reconnaissance Orbiter (MRO)/Mars Climate Sounder (MCS) temperatures at 80 km (panel b) around the equator (±15° latitude) for sols 597–615. The ultra-fast Kelvin wave peak at 1.4 cycles (marked as a solid black diamond) and the sideband peaks at 0.6 (marked as 2^-), 1.6 (marked as 3^-), 2.4 (marked as 1^+), and 3.4 (marked as 2^+) cycles are all evident both at 80 and 150 km.

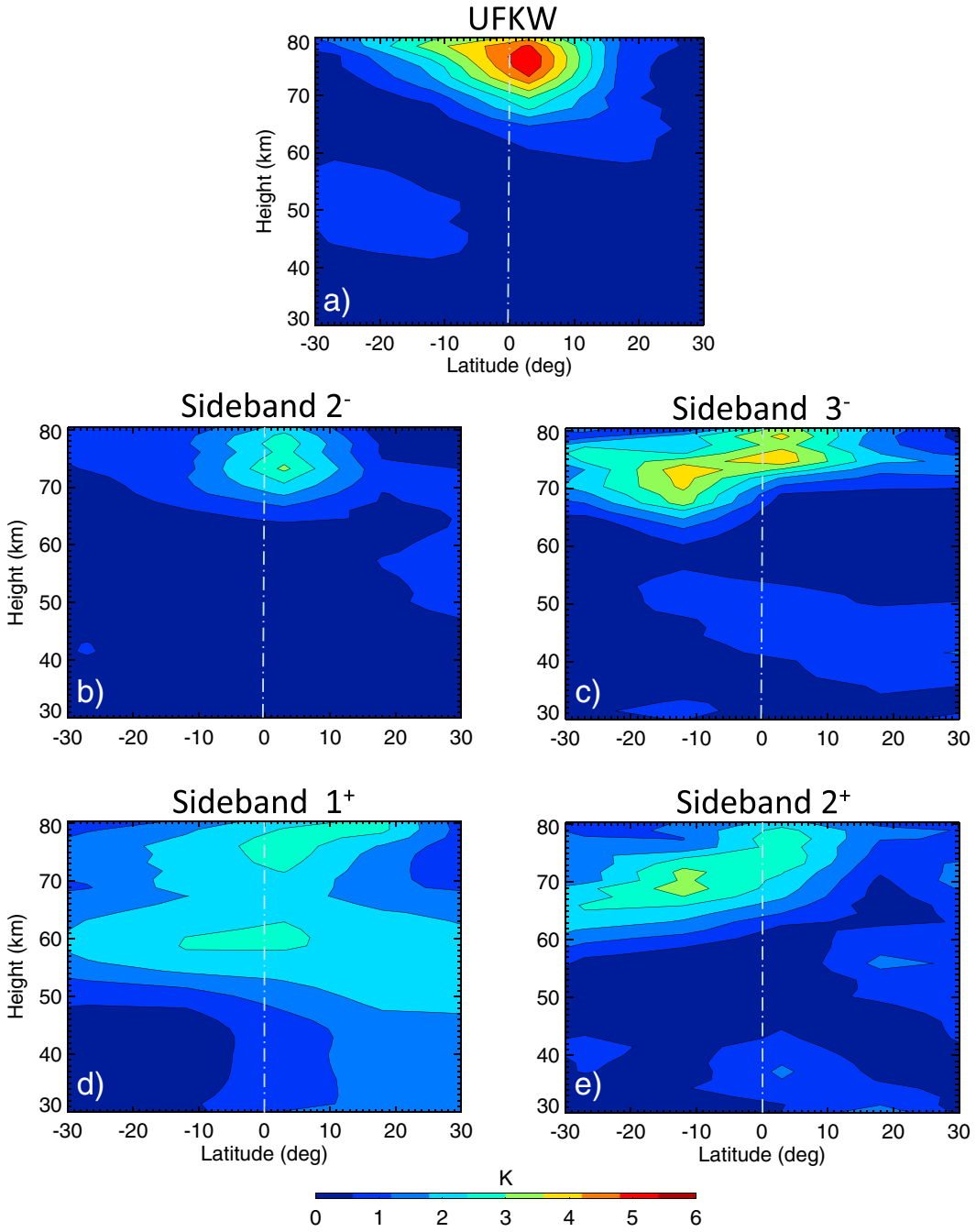

Figure 5. Height (30–80 km) versus latitude (±30°) depiction of ultra-fast Kelvin wave (UFKW; panel a), sideband 2^- (panel b), sideband 3^- (panel c), sideband 1^+ (panel d), and sideband 2^+ (panel e) temperature amplitudes from Mars Reconnaissance Orbiter/Mars Climate Sounder for sols 597–615.

with periods of 3.5–5 sols and $s = 0, 2$ that are found in the spectra at 80 km are not observed at 150 km. These waves likely dissipate between 80 and 150 km. The spectrum in Figure 3*a*′ also shows $s = -1$ periodicities around 3 sols and 4.5 sols that, although less prominent, are also present in Figure 3*b*′. These longer period UFKWs possess comparatively small amplitudes and are not addressed further.

The pseudolongitude spectra of MAVEN ZMR density residuals at 150 km (Figure 4a) and MCS ZMR temperatures at 80 km (Figure 4b) show the 1.4-cycle signature due to the 2.5-sol UFKW (note that a UFKW with zonal wavenumber $m = -1$ and frequency $\delta\Omega = 0.4$ sol^{-1} yields a peak in a pseudolongitude spectrum at $| m - \delta | = | -1 - 2.5^{-1} | = 1.4$.). At 80 km there are strong peaks around 1 cycle (i.e., longitudinal wave-1 as seen

from Sun-synchronous orbit), 2 cycles (i.e., wave-2), and 3 cycles (i.e., wave-3), while at 150 km there are only peaks around 1 cycle and 2 cycles associated with wave-1 and wave-2, respectively. The diurnal eastward tide with $s = -1$ (i.e., DE1 or DK1) is likely the main contributor to the observed wave-2 structure (e.g., Angelats i Coll et al., 2004; Bougher et al., 2004; Wilson, 2002; Withers et al., 2003, 2011); the wave-3 structure, which is typically weaker than the wave-2 component, can be attributed to the diurnal eastward tide with $s = -2$ (i.e., DE2 or DK2; Guzewich et al., 2012; Wolkenberg & Wilson, 2014); while the wave-1 component, which is typically weaker than both wave-2 and wave-3, is likely associated with the diurnal stationary tide (D0) and the semidiurnal westward $s = 1$ tide (SW1; Moudden & Forbes, 2008). Lack of wave-3 at 150 km suggests dissipation of DE2 between 80 and 150 km. This is in contrast with results from the Mars Climate Database analyzed by us (not shown), and Moudden and Forbes (2015), that indicate large DE2 amplitudes around 150 km and thus warrants further investigation.

Also clearly identifiable and labeled in Figure 4 are the sideband peaks at 0.6 cycles (2^-), 1.6 cycles (3^-), 2.4 cycles (1^+), and 3.4 cycles (2^+) arising from the interaction between the UFKW and the solar tides. (In the notation A^b, A denotes the interacting wave [i.e., wave-1, wave-2, or wave-3)], while b specifies whether it is the sum [i.e., $b = \}+'$] or the difference ($b = \}-'$) sideband). The SW peaks at 0.6 and 3.4 cycles are likely a result of the interaction between the UFKW and DE1, the peak at 1.6 cycles is likely the signature of the interaction of the UFKW with DE2, while the peak at 2.4 cycles is likely arising from the interaction of the UFKW with D0 and/or SW1. As demonstrated by Figure 4, the large majority of the longitudinal variability at both heights is associated with solar tides, the UFKW, and their nonlinear interactions. Other notable peaks in the spectra around 0.11 and 0.20 cycles of the tidal peaks are indicative of 5-sol and 9-sol modulations. Identification of the specific tidal components involved in the interaction is beyond the scope of the current investigation. A follow-on study will encompass these attributions along with correlative analyses of longer period PWs.

The height-latitude structure of the UFKW and sidebands 2^-, 3^-, 1^+, 2^+ between $\pm 30°$ latitude and extending from 30 to 80 km retrieved using the pseudolongitude spectral peaks in MCS ZMR temperatures is presented in Figure 5. The UFKW is found to maximize around 78 km and possess amplitudes up to 6 K, while the sidebands are found to maximize around 70–75 km (2^-, 3^-), 60–70 km (1^+), and 68 km (2^+) with amplitudes up to 4 K. The UFKW and the 2^- sideband are mostly equatorially symmetric, while the sidebands 3^-, 1^+, and 2^+ display significant latitudinal asymmetry possibly due to tidal structures that are not purely symmetric (e.g., Moudden & Forbes, 2015) and/or to the effect of mean winds and dissipation (e.g., Gasperini, Forbes, & Hagan, 2017). Figure 5 also shows that the UFKW is mainly confined to a narrow latitude band of $\pm 15°$ around of the equator, while the sidebands can extend up to $\sim \pm 30°$ latitude.

5. Summary and Conclusions

In this work we examined concurrent temperature measurements from MRO/MCS around 80 km and neutral density measurements from MAVEN's accelerometer near periapsis (i.e., ~130–170 km) between 1 November 2014 and 31 April 2017 to reveal evidence of a strong 2.5-sol UFKW in the middle and upper atmosphere of Mars near autumnal equinox. We further demonstrated the existence of SWs generated by nonlinear interactions between the UFKW and the solar tides and show that these SWs represent a significant source of variability in Mars' middle and upper atmosphere. Analyzing MCS temperatures around 30–80 km we demonstrated that the UFKW maximizes around 78 km and possesses amplitudes of up to 6 K, while the sidebands peak near 60–75 km with amplitudes of up to 4 K. Examining the height-latitude structure of the UFKW and the SWs we find that the UFKW is quasi-symmetric about the equator and confined to a narrow latitude band of $\pm 15°$ around the equator, while the SWs can extend up to $\sim \pm 30°$ latitude and possess significant latitudinal asymmetry likely due to tidal modes that are not purely symmetric and/or to the effects of wave dissipation and background winds.

Our study suggests that the 2.5-sol UFKW and SWs generated by its interaction with solar tides may contribute to the longitudinal variability in Mars' aerobraking region. In a follow-on study we plan to extend the analysis of nonlinear interactions to longer period PWs, for example, 5-sol and 9-sol waves, and study seasonal effects and variability at UFKW periods (2–6 days) using MCS data. We will further investigate solar irradiance effects in Mars' upper atmosphere using in situ measurements made by the MAVEN EUV monitor. This correlative analysis will enable us to estimate the relative contribution of upward propagating waves and solar forcing in generating sol-to-sol variability in Mars aerobraking region.

Acknowledgments
The MRO/MCS temperature data used in this study (version v4) can be accessed from the Derived Data Record archive available at the Planetary Science Database (http://pds-atmospheres.nmsu.edu/), while the MAVEN neutral density data can be downloaded from the Science Data Center at the Laboratory for Atmospheric and Space Physics (https://lasp.colorado.edu/maven/sdc). The efforts of Federico Gasperini and Maura E. Hagan were supported by a seed grant from the Office of Research and Graduate Studies (ORGS) at Utah State University. Jeffrey M. Forbes acknowledges support under NASA MDAP Award NNX16AJ39G.

References

Angelats i Coll, M., Forget, F., Lopez-Valverde, M. A., Read, P. L., & Lewis, S. R. (2004). Upper atmosphere of Mars up to 120 km: Mars Global Surveyor accelerometer data analysis with the LMD general circulation model. *Journal of Geophysical Research*, *109*, E01011. https://doi.org/10.1029/2003JE002163

Bougher, S. W., Blelly, P.-L., Combi, M., Fox, J. L., Mueller-Wodarg, I., Ridley, A., & Roble, R. G. (2008). Neutral upper atmosphere and ionosphere modeling. *Space Science Reviews*, *139*, 107–141. https://doi.org/10.1007/s11214-008-9401-9

Bougher, S. W., Engel, S., Hinson, D. P., & Murphy, J. R. (2004). MGS Radio Science electron density profiles: Interannual variability and implications for the Martian neutral atmosphere. *Journal of Geophysical Research*, *109*, E03010. https://doi.org/10.1029/2003JE002154

Breus, T. K., & Krymskii, A. M. (2017). Remnant magnetic fields of Mars and their interaction with the solar wind. *Cosmic Research*, *55*, 235–247. https://doi.org/10.1134/S0010952517040025

Cahoy, K. L., Hinson, D. P., & Tyler, G. L. (2006). Radio science measurements of atmospheric refractivity with Mars Global Surveyor. *Journal of Geophysical Research*, *111*, E05003. https://doi.org/10.1029/2005JE002634

England, S. L., Liu, G, Withers, P, Yiğit, E., Lo, D., Jain, S., et al. (2016). Simultaneous observations of atmospheric tides from combined in situ and remote observations at Mars from the MAVEN spacecraft. *Journal of Geophysical Research: Planets*, *121*, 594–607. https://doi.org/10.1002/2016JE004997

Forbes, J. M. (2002). Wave coupling in terrestrial planetary atmospheres. In M. Mendillo, A. Nagy, & J. H. Waite (Eds.), *Atmospheres in the solar system: Comparative aeronomy, Geophysical Monograph Series* (Vol. 130, pp. 171–190). Washington, DC: American Geophysical Union.

Forbes, J. M., Bridger, A. F. C., Bougher, S. W., Hagan, M. E., Hollingsworth, J. L., Keating, G. M., & Murphy, J. (2002). Nonmigrating tides in the thermosphere of Mars. *Journal of Geophysical Research*, *107*(E11), 5113. https://doi.org/10.1029/2001JE001582

Forbes, J. M., Bruinsma, S., & Lemoine, F. G. (2006). Solar rotation effects on the thermospheres of Mars and Earth. *Science*, *312*, 1366–1368. https://doi.org/10.1126/science.1126389

Forbes, J. M., & Hagan, M. E. (2000). Diurnal Kelvin wave in the atmosphere of Mars: Towards an understanding of 'stationary' density structures observed by the MGS accelerometer. *Geophysical Research Letters*, *27*(21), 3563–3566.

Forbes, J. M., Hagan, M. E., Bougher, S. W., & Hollingsworth, J. L. (2001). Kelvin wave propagation in the upper atmospheres of Mars and Earth. *Advances in Space Research*, *27*(11), 1791–1800. https://doi.org/10.1016/S0273-1177(01)00286-1

Forbes, J., Zhang, X., Maute, A., & Hagan, M. E. (2018). Zonally-symmetric oscillations of the thermosphere at planetary-wave periods. *Journal of Geophysical Research*, *123*. https://doi.org/10.1002/2018JA025258

Forget, F., Hourdin, F., Fournier, R., Hourdin, C., Talagrand, O., Collins, M., et al. (1999). Improved general circulation models of the Martian atmosphere from the surface to above 80 km. *Journal of Geophysical Research*, *104*(E10), 24,155–24,175. https://doi.org/10.1029/1999JE001025

Gasperini, F., Forbes, J. M., Doornbos, E. N., & Bruinsma, S. L. (2015). Wave coupling between the lower and middle thermosphere as viewed from TIMED and GOCE. *Journal of Geophysical Research: Space Physics*, *120*, 5788–5804. https://doi.org/10.1002/2015JA021300

Gasperini, F., Forbes, J. M., Doornbos, E. N., & Bruinsma, S. L. (2017). Kelvin wave coupling from TIMED and GOCE: Inter/intra-annual variability and solar activity effects. *Journal of Atmospheric and Solar-Terrestrial Physics*, *171*, 176–187. https://doi.org/10.1016/j.jastp.2017.08.034

Gasperini, F., Forbes, J. M., & Hagan, M. E. (2017). Wave coupling from the lower to the middle thermosphere: Effects of mean winds and dissipation. *Journal of Geophysical Research: Space Physics*, *122*, 7781–7797. https://doi.org/10.1002/2017JA024317

Guzewich, S. D., Talaat, E. R., & Waugh, D. W. (2012). Observations of planetary waves and nonmigrating tides by the Mars Climate Sounder. *Journal of Geophysical Research*, *117*, E03010. https://doi.org/10.1029/2011JE003924

Jakosky, B. M., Grebowsky, J. M., Luhmann, J. G., & Brain, D. A. (2015). Initial results from the MAVEN mission to Mars. *Geophysical Research Letters*, *42*, 8791–8802. https://doi.org/10.1002/2015GL065271

Jakosky, B. M., Slipski, M., Benna, M., Mahaffy, P., Elrod, M., Yelle, R., et al. (2017). Mars' atmospheric history derived from upper-atmospheric measurements of $^{38}Ar/^{36}Ar$. *Science*, *355*, 1408–1410. https://doi.org/10.1126/science.aai7721

Liu, G., England, S., Lillis, R. J., Mahaffy, P. R., Elrod, M., Benna, M., & Jakosky, B. (2017). Longitudinal structures in Mars' upper atmosphere as observed by MAVEN/NGIMS. *Journal of Geophysical Research: Space Physics*, *122*, 1258–1268. https://doi.org/10.1002/2016JA023455

Longuet-Higgins, M. S. (1968). The eigenfunctions of Laplace's tidal equation over a sphere. *Philosophical Transactions of the Royal Society of London*, *262*, 511–607.

McCleese, D. J., Schofield, J. T., Taylor, F. W., Calcutt, S. B., Foote, M. C., Kass, D. M., et al. (2007). Mars Climate Sounder: An investigation of thermal and water vapor structure, dust and condensate distributions in the atmosphere, and energy balance of the polar regions. *Journal of Geophysical Research*, *112*, E05S06. https://doi.org/10.1029/2006JE002790

Millour, E., Forget, F., Spiga, A., Navarro, T., Madeleine, J.-B., Montabone, L., et al. (2015). The Mars Climate Database (MCD version 5.2). European Planetary Science Congress 2015, vol. 10, EPSC2015-438, Nantes, France, 27 Sept.-2 Oct.

Moudden, Y., & Forbes, J. M. (2008). Topographic connections with density waves in Mars' aerobraking regime. *Journal of Geophysical Research*, *113*, E11009. https://doi.org/10.1029/2008JE003107

Moudden, Y., & Forbes, J. M. (2010). A new interpretation of Mars aerobraking variability: Planetary wave-tide interactions. *Journal of Geophysical Research*, *115*, E09005. https://doi.org/10.1029/2009JE003542

Moudden, Y., & Forbes, J. M. (2011a). First detection of wave interactions in the middle atmosphere of Mars. *Geophysical Research Letters*, *38*, L04202. https://doi.org/10.1029/2010GL045592

Moudden, Y., & Forbes, J. M. (2011b). Simulated planetary wave-tide interactions in the atmosphere of Mars. *Journal of Geophysical Research*, *116*, E01004. https://doi.org/10.1029/2010JE003698

Moudden, Y., & Forbes, J. M. (2013). A decade-long climatology of terdiurnal tides using TIMED/SABER observations. *Journal of Geophysical Research: Space Physics*, *118*, 4534–4550. https://doi.org/10.1002/jgra.50273

Moudden, Y., & Forbes, J. M. (2015). Density prediction in Mars' aerobraking region. *Space Weather*, *13*, 86–96. https://doi.org/10.1002/2014SW001121

Palo, S. E., Roble, R. G., & Hagan, M. E. (1999). Simulation of the quasi-two-day wave using the TIME-GCM: Dynamical effects in the middle atmosphere. *Earth Planets Space*, *51*, 629–647.

Teitelbaum, H., & Vial, F. (1991). On tidal variability induced by nonlinear interaction with planetary waves. *Journal of Geophysical Research*, *96*(A8), 14169–14178. https://doi.org/10.1029/91JA01019

Wang, L., Fritts, D. C., & Tolson, R. H. (2006). Nonmigrating tides inferred from the Mars Odyssey and Mars Global Surveyor aerobraking data. *Geophysical Research Letters*, *33*, L23201. https://doi.org/10.1029/2006GL027753

Wilson, R. J. (2000). Evidence for diurnal period Kelvin waves in the Martian atmosphere from Mars Global Surveyor TES data. *Geophysical Research Letters*, *27*(23), 3889–3892. https://doi.org/10.1029/2000GL012028

Wilson, R. J. (2002). Evidence for nonmigrating thermal tides in the Mars upper atmosphere from the Mars Global Surveyor Accelerometer Experiment. *Geophysical Research Letters*, *29*(7), 1120. https://doi.org/10.1029/2001GL013975

Withers, P., Bougher, S. W., & Keating, G. M. (2003). The effects of topographically-controlled thermal tides in the Martian upper atmosphere as seen by the MGS accelerometer. *Icarus*, *164*, 14–32. https://doi.org/10.1016/S0019-1035(03)00135-0

Withers, P., Pratt, R., Bertaux, J.-L., & Montmessin, F. (2011). Observations of thermal tides in the middle atmosphere of Mars by the SPICAM instrument. *Journal of Geophysical Research*, *116*, E11005. https://doi.org/10.1029/2011JE003847

Wolkenberg, P., & Wilson, R. J. (2014). Mars Climate Sounder observations of wave structure in the north polar middle atmosphere of Mars during the summer season. Pasadena, CA.

Zurek, R., Tolson, R., Baird, D., Johnson, M. Z., & Bougher, S. W. (2015). Application of MAVEN accelerometer and attitude control data to Mars atmospheric characterization. *Space Science Reviews*, *195*, 303–317. https://doi.org/10.1007/s11214-014-0095-x

Zurek, R. W., Tolson, R. A., Bougher, S. W., Lugo, R. A., Baird, D. T., Bell, J. M., & Jakosky, B. M. (2017). Mars thermosphere as seen in MAVEN accelerometer data. *Journal of Geophysical Research: Space Physics*, *122*, 3798–3814. https://doi.org/10.1002/2016JA023641